

Low-Birefringent, Chiral Banana Phase below Calamitic Nematic and/or Smectic C Phases in Oxadiazole Derivatives

Sungmin Kang, Yuki Saito, Nobuhiro Watanabe, Masatoshi Tokita, Yoichi Takanishi, Hideo Takezoe, and Junji Watanabe*

Department of Organic and Polymeric Materials, Tokyo Institute of Technology, Ookayama, Meguro-ku, Tokyo 152, Japan

Received: December 14, 2005; In Final Form: January 26, 2006

Bent-shaped molecules based on the oxadiazole central core with various side wings and terminal chain groups have been synthesized, and their liquid-crystalline behavior was investigated by optical microscopic, X-ray, and electrooptic measurements. These molecules exhibit liquid-crystal polymorphism including both the calamitic and banana phases. Such a characteristic polymorphism is attributable to the larger bend angle of the oxadiazole core compared to that of the resorcinol core used in conventional banana molecules. Only one type of banana phase, designated as the Bx phase, is formed. It appears upon cooling from the nematic and smectic liquid crystals and exhibits chiral domains with a very weak birefringence (apparently optically isotropic). By applying an electric field, the Bx phase is altered to a high-birefringence B2 phase with a homochiral SmC_AP_A structure that exhibits an antiferroelectric response. From detailed analyses of the optical texture and X-ray patterns through the transformation from well-oriented calamitic phases, the Bx phase was found to exhibit a helical structure, which arises as a frustration from the ground-state B2 phase in such a manner that the blocks of B2 layers are twisted with respect to each other in a direction parallel to the layer plane similarly to the twisted grain boundary (TGB) phase.

Introduction

The shape of a molecule has a critical effect on liquid crystallinity, and the linearity of molecules has been considered to provide an advantage in the formation of mesophases in calamitic liquid crystals. However, since the earlier studies of nonlinear mesogens by Vorländer¹ and Demus,² many new materials with nonlinear architecture mesogens have been found to exhibit mesophases. One of these is the bent-shaped molecules that have been synthesized and reported to form mesophases by Matsunaga et al.^{3–5}

On the other hand, Watanabe et al.^{6–8} found that there is a bent (alternately tilted) alignment of mesogens in the smectic CA phase formed from main-chain liquid-crystal polymers. This distinct alignment is caused by a conformational constraint of the flexible spacer joining the mesogens. Following this, they suggested that the main-chain polymers would form ferroelectric smectic liquid crystals even in an achiral system by considering the packing symmetry of bent molecules.⁸ After investigating several materials,^{9–13} they obtained exotic banana-shaped molecules, 1,3-benzene bis[4-(4-n-alkoxyphenylinominomethyl)-benzoate] (P-n-O-PIMB), based on a resorcinol core¹⁴ that clearly form ferroelectric and antiferroelectric smectic liquid crystals. Further extensive research into banana molecules led to another interesting finding that the P-n-O-PIMB molecules can form chiral phases even in achiral molecular systems. A typical phase is the low-temperature B4 phase, which shows two chiral domains with opposite optical rotations.¹⁵ Thus, ferroelectricity and chirality have been topical features for these sorts of achiral bent-shaped materials.^{16–19} Through these studies, the initially treated P-n-O-PIMB molecules have

played the role of a parent compound for many other novel banana molecules.

More recently, Samulski et al. also reported a molecular system of nonlinear mesogens having heterocyclic cores that can provide a more moderate bending angle than the resorcinol core.^{20,21} In these reports, an oxadiazole core was used as one of the heterocyclic cores, and their liquid crystallinity was examined by focusing on the biaxiality in smectic and nematic phases.^{22,23} In our recent study, we found that the oxadiazole-based molecules exhibit an interesting polymorphism in which the banana Bx phase is formed in the lower-temperature region than well-known calamitic phases, that is, nematic, SmA, and SmC phases. Such a polymorphism including both types of banana and calamitic liquid crystals is attributed to the moderate bend angle of oxadiazole cores. Of interest is the finding that the Bx phase is a fluid smectic phase that is essentially chiral and optically isotropic. Recently, such peculiar characteristics of the banana phase have become noteworthy. In this study, we examined the phase structure of the banana Bx phase in relation to the well-defined structure of calamitic phases that existed before.

Synthesis

Syntheses along with analytical data for 2,5-bis-(*p*-hydroxyphenyl)-1,3,4-oxadiazole and its derivatives, which are the prototypes of our materials, have already been reported by Samulski et al.^{20,21}

A synthesis scheme for one representative compound, 2,5-bis(*p*-nonaloyloxybiphenyl)-1,3,4-oxadiazole (ODBP), among the compounds being introduced here is illustrated in Scheme 1 (1–5).

4'-Acetoxybiphenyl-4-benzoic Acid (1). 4'-Hydroxybiphenyl-4-benzoic acid (20 mmol) and acetic anhydride (50 mmol)

* Corresponding author. E-mail: jwatanab@polymer.titech.ac.jp.

SCHEME 1

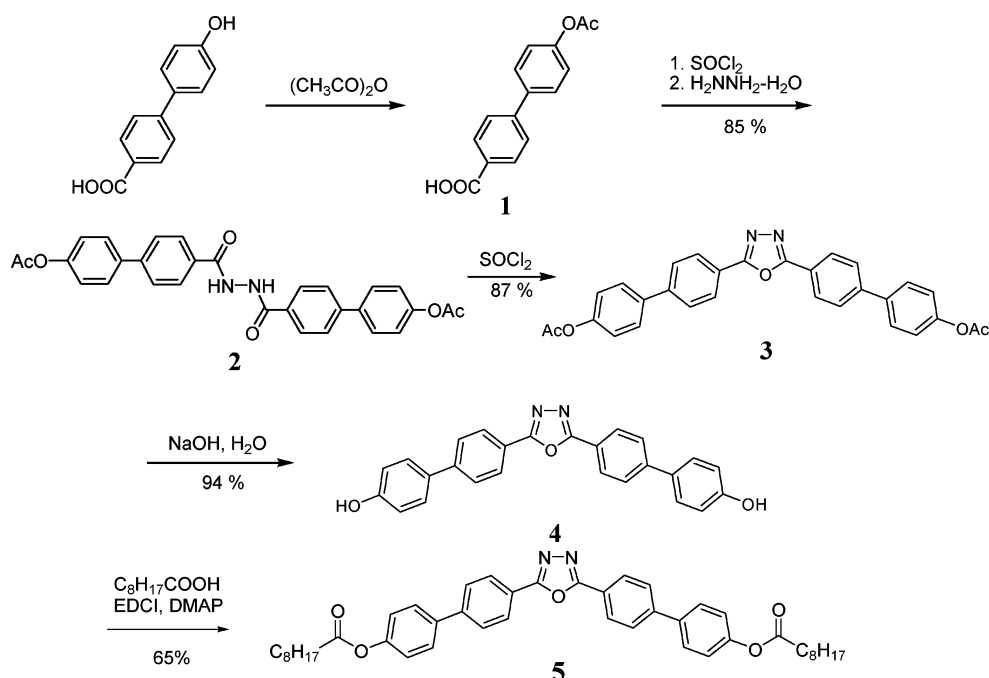


TABLE 1: Phase Transition Behavior of the Oxadiazole and Thiadiazole Derivatives

Compound	Molecular Structure	Transition sequence Temperature ($^{\circ}C$) and Enthalpy ($-k\text{J mol}^{-1}$)
(a) ODP-OCO-8		Cr _{(88) (16.1)} BX _{(114) (23.5)} Iso
(b) ODBP-OCO-8		Cr ₂ _{(99) (11.2)} Cr ₁ _{(191) (6.0)} BX _{(251) (9.5)} N _{(261) (2.1)} Iso
(c) TDP-OCO-8		Cr ₃ _{(80) (3.3)} Cr ₂ _{(94) (20.5)} Cr ₁ _{(107) (10.3)} SmC _{(207) (8.8)} Iso
(d) TDBP-OCO-8		Cr _{(200) (17.1)} SmC ₍₃₀₀₎ (decomposition) ^a

^a Phase sequence determined upon heating.

in tetrahydrofuran (THF) with pyridine were stirred for 12 h at room temperature. After agitation, pure water and hydrochloric acid (HCl) were added, and the precipitate was filtered. The resulting solid was washed with pure water and ethanol for the next reaction.

1,2-(*p*-Acetoxybiphenyl)hydrazine (2). 4'-Acetoxybiphenyl-4-benzoic acid (**1**) (18.7 mmol) and thionyl chloride (20 mL) with small drops of dimethylformamide (DMF) were refluxed for 3 h at 50 °C. 4'-Acetoxybiphenyl-4-benzoic chloride was obtained by removing the remaining unreacted thionyl chloride after the reaction. Then, 4'-acetoxybiphenyl-4-benzoic chloride and hydrazine hydrate (8.4 mmol) in THF (40 mL) with trimethylamine (8.4 mmol) were stirred for 12 h at room temperature. After agitation, the precipitate was filtered and washed with chloroform.

2,5-Bis(*p*-acetoxybiphenyl)-1,3,4-oxadiazole (3). 1,2-(*p*-Acetoxybiphenyl)hydrazine (**2**, 7.09 mmol) was refluxed with thionyl chloride (30 mL) for 3 h. After completion of the

reaction and removal of unreacted thionyl chloride, the target compound was obtained by recrystallizing the resulting solid from acetone.

2,5-Bis(*p*-hydroxybiphenyl)-1,3,4-oxadiazole (4). 2,5-Bis(*p*-acetoxybiphenyl)-1,3,4-oxadiazole (**3**) was dissolved in ethanol and stirred for 1 h with sodium hydroxide solution. After agitation, a dilute HCl solution was added, and the resulting precipitate was obtained by filtration.

2,5-Bis(*p*-nonaloyloxybiphenyl)-1,3,4-oxadiazole (ODBP) (5). ODBP compounds were prepared by condensation reaction of compound **4** and *n*-carboxylic acids with various carbon numbers by stirring for 24 h at room temperature in anhydrous chloroform containing 1-ethyl-3,3-dimethylaminopropyl carbodiimide hydrochloride (EDCI) and (dimethylamino)pyridine (DMAP). Finally, ODBP compounds were obtained by purifying the crude product with gel permeation chromatography and recrystallization from chloroform/ethanol.

Experiments

Polarized optical microscopic (POM) measurements were performed using an Olympus BX50 polarizing microscope equipped with a temperature-controlled Mettler Toledo FP82 hot stage. The transition temperatures and corresponding enthalpies were determined using a differential scanning calorimeter (Perkin-Elmer, Pyris1 DSC).

Wide-angle X-ray diffraction (WAXD) measurements were obtained using a Rigaku R-200 diffractometer with Cu K α radiation. Microbeam X-ray experiments were performed on beamline 4A (BL-4A) of Photon Factory (PF), Tsukuba, Japan. The beam size is roughly $3 \times 4 \mu\text{m}^2$, and the energy is 8 keV. The diffraction pattern was recorded using a two-dimensional area detector. The homeotropic sample for X-ray measurements was prepared on a glass substrate that was coated with commercially available organosilane *N,N*-dimethyl-*n*-octadecyl-3-aminopropyltrimethoxysilyl chloride (DMOAP). The sample was then heated to the isotropic melt and cooled to the smectic phase at a rate of 1°C min^{-1} . By this procedure, the alkyl end groups of the molecules interact closely with the octadecyl group of the organosilane compound covalently linked to the glass surface, resulting in the homeotropic orientation of the nematic and smectic phases.

Electrooptic switching was observed using a high-speed amplifier (FLC Electronics, F20A) connected to a function generator (NF Electronic Instruments, 1945A). For these measurements, the sample was sandwiched between two glass plates with a transparent indium tin oxide (ITO) electrode and with the rubbed polyimide layers for obtaining homogeneously aligned domains. The cell gap was controlled to be $5 \mu\text{m}$ using poly(ethylene terephthalate) (PET) films.

The temperature was regulated with an accuracy of $\pm 0.2^\circ\text{C}$ using a Mettler FP-82 controller for all measurements.

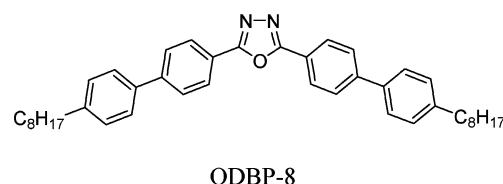
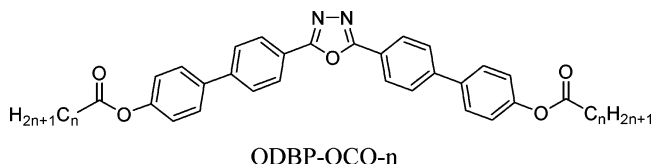
Results and Discussion

1. Effect of Central Bent-Core Moieties with Different Bend Angles on Liquid-Crystalline Behavior. First, we examined the liquid crystallinity in four kinds of compounds in which the side wings are terminated by octyl chains via the ester linkage. Two of them, ODP-OCO-8 and ODBP-OCO-8, have the oxadiazole central ring and two types of side wings that are phenyl and biphenyl moieties, respectively. The other two materials, TDP-OCO-8 and TDBP-OCO-8, are based on the thiadiazole core. These are listed in Table 1, along with their mesomorphic sequences. Through these modifications, which were intended for examining the effect of central rings and side wings, we can first see a huge increase of transition temperatures for compounds with longer biphenyl side wings. For example, the replacement of a phenyl by a biphenyl side wing increases the isotropization temperature by about 150°C , as found for the oxadiazole derivatives. On the other hand, the mesomorphic nature is affected by the central ring rather than the side wing. The thiadiazole derivatives hold only the calamitic SmC phase, whereas the oxadiazole derivatives exhibit a bimorphism in which an undesigned banana phase, the so-called Bx phase, appears below the typical nematic phase. Formation of the banana phase in the oxadiazole derivatives can be interpreted as an effect of the bend angle produced by the central core unit. If the bend angle is simply designated as an angle between two bonds sticking out of the central core, the oxadiazole derivative has a bend angle of about 135° , which is slightly larger than that (120°) of the classic banana molecules based on the resorcinol core.²⁴ On the other hand, the thiadiazole

moiety gives a larger bend angle ($\sim 160^\circ$), and so its derivatives seem to behave like conventional rod-shaped molecules. The larger bend angle also reflects on the isotropization temperature (T_i) of the mesophase: the thiadiazole derivatives show fairly higher T_i values than the oxadiazole derivatives. Thus, we conclude that bend angles of 120° to 135° are responsible for the formation of the banana phases.

2. Effect of Linkage Group and Length of Terminal Alkyl Chain on Liquid-Crystalline Behavior in ODBP Homologues. The oxadiazole derivatives, showing a polymorphism including both the banana and calamitic mesophases, are of great interest because the structure of banana phases can be examined in relation to the well-defined structure of calamitic liquid crystals.^{25,26}

To comprehend more details of the polymorphism in the oxadiazole derivatives, we prepared here three different homologues of ODBP with different terminal units, namely, alkylester, alkyl ether, and alkyl units. The chemical structures of these homologues, abbreviated here as ODBP-OCO-*n*, ODBP-O-*n*, and ODBP-8, respectively, are given below.



2.1. ODBP-OCO-*n* with *n* = 7–15. The thermodynamic data and phase transition behavior of the ODBP-OCO-*n* series are listed in Table 2 and shown in Figure 1a. As mentioned above, polymorphism is clearly observed, with the nematic and SmC phases in a higher-temperature region and the Bx phase in a lower-temperature region. As the terminal chain length is increased, the nematic regime becomes narrower, and so the SmC regime is expanded. This is a typical trend caused by a preferred segregation of mesogenic and aliphatic units. The Bx phase is located in the wide temperature region until the crystallization takes place.

For all of the prepared homologues, the Bx phase shows an undefined texture with very weak birefringence. Further, note that two types of optically active domains with opposite chirality are formed, exchanging brightness with the rotation of the polarizer against the analyzer either clockwise or anticlockwise (see later). Wide-angle X-ray diffraction measurements exhibit an inner sharp layer reflection and an outer broad reflection, indicating that the molecules are packed into a layer with a liquidlike in-plane order. When it appears from the SmC phase, its layer spacing is equivalent to that of the SmC phase for every

TABLE 2: Phase Transition Temperatures ($^{\circ}$ C) and Enthalpies ($-k\text{J mol}^{-1}$) of ODBP–OCO-*n* Determined upon Cooling

<i>n</i>	Cr	Bx	SmC	N	Iso
7	● 193 7.5	● 252 9.3		● 266 2.6	●
8	● 191 6.0	● 251 9.5		● 261 2.1	●
9	● 185 7.0	● 246 10.9	● 250 2.5	● 256 3.6	●
10	● 185 9.5	● 239 9.6	● 242 7.5		●
11	● 181 8.8	● 236 6.9	● 246 6.9		●
12	● 184 8.4	● 233 5.6	● 246 7.1		●
13	● 182 7.0	● 227 4.1	● 241 5.8		●
15	● 175 9.2	● 214 4.5	● 231 7.9		●

compound (see Table 3). From a comparison of the layer spacings with the molecular lengths, the tilt angles of the molecules in these Bx and SmC phases are found to be 28–34°. Thus, in terms of the X-ray data, there is no apparent difference between the Bx and SmC phases, although the microscopic texture is completely different between the two. The detailed structure and properties of the Bx phase are shown later.

2.2. ODBP–O-*n* with *n* = 6–15. As can be seen in Figure 1b, the ODBP–O-*n* series shows a significantly different mesomorphic behavior than the ODBP–OCO-*n* series. The Bx phase completely disappears, and only calamitic mesophases can be observed. Comparing the phase behavior of these two series, we find that the crystal melting temperature is fairly high in the ODBP–O-*n* homologues.

2.3. ODBP-8. The only prepared material in this system is ODBP-8, which shows the phase sequence (the transition enthalpies within parentheses are given in kJ mol^{-1} units),

Iso 221 $^{\circ}$ C (3.6) SmA 200 $^{\circ}$ C (8.6) Bx 69 $^{\circ}$ C (8.9) Cr

Here, the Bx phase also appears with an undefined and weakly birefringent texture similarly to the ODBP–OCO-*n* homologues. The layer spacing of the Bx phase is 29.5 \AA , which is markedly smaller than the 38.0 \AA of the SmA phase. This is direct evidence for the tilting of molecules to the layer normal in the Bx phase. The tilt angle is estimated to be 35°.

Through this systematic study on three series, we know that the formation of the Bx phase depends on the terminal linkage moiety. The Bx phase is formed from ODBP–OCO-*n* and ODBP-8, but not from ODBP–O-*n*. However, this seems not to indicate that ODBP–O-*n* molecules do not exhibit the potentiality for Bx phase formation. Considering that the crystallization temperatures ranging from 200 to 230 $^{\circ}$ C in ODBP–O-*n* are appreciably higher than those of 170 to 190 $^{\circ}$ C in ODBP–OCO-*n*, the absence of the Bx phase in ODBP–O-*n* series can be attributed to an easy crystallization occurring before the Bx phase appears.

3. Struture and Properties of the Bx Phase. Recently, the fluid Bx phase, which appears as undefined texture with a fairly low birefringence or optically isotropic texture, has become noteworthy. The first such phase was reported as Sm1 by Thisayukta et al.,²⁷ and then several reports have been

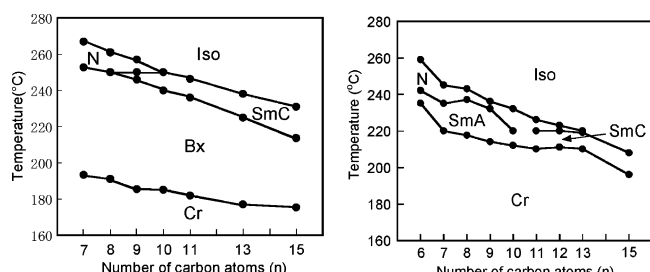


Figure 1. Phase transition behavior observed for (a) ODBP–OCO-*n* and (b) ODBP–O-*n*.

TABLE 3: Layer Spacings of the SmC and Bx Phases and Their Tilt Angles Calculated in a Comparison of the Molecular Lengths for ODBP–OCO-*n*

<i>N</i>	layer spacing (\AA)		molecular length ^a (\AA)	tilt angle (deg)
	SmC	Bx		
7	—	32.6	36.9	28
8	—	33.3	38.4	30
9	35.1	34.9	41.2	32
10	36.6	36.6	42.7	31
11	38.0	37.9	45.5	34
12	39.5	39.5	47.0	33
13	41.6	41.4	49.8	34

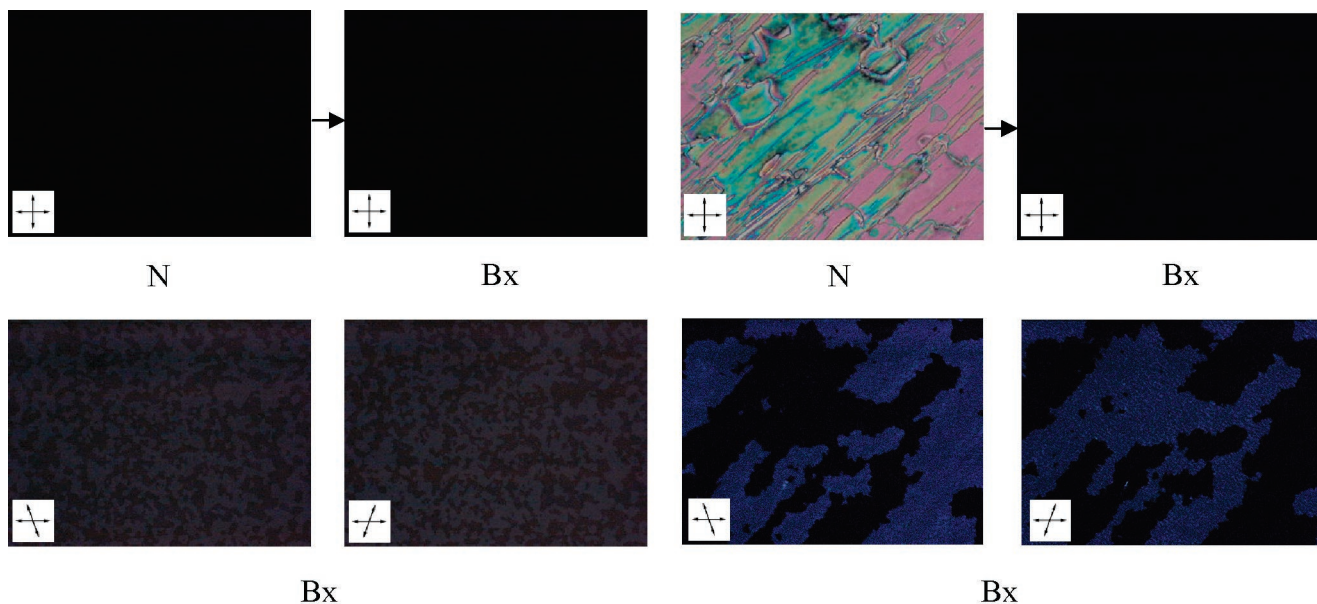
^a Calculated molecular lengths are based on the most extended chains.

made.^{26,28–39} Another remarkable feature of this Bx phase being reported in the literature is to show a spontaneous separation of two chiral domains with opposite optical rotations under polarized optical microscopic observation, which is similar to the solid B4 phase.¹⁸ It is also reported that the Bx phase can be induced by an application of external electric fields to the B2 phase.^{33–35}

The present homologous series of ODBP materials that form the Bx phase, as well as the nematic, smectic A, and smectic C phases, are especially interesting because the well-developed monodomain structure of these calamitic phases can be easily prepared by the conventional methods such as the rubbing treatment, and then the structural details of the Bx phase can be determined through analyses of structural changes during their transformation to the Bx phase.

Figure 2 shows the POM textures for the Bx phase of ODBP–OCO-8 transformed from the nematic phase. It is optically isotropic or weakly birefringent under crossed polarization. By the rotation of polarizer, the two chiral domains of the Bx phase with opposite optical rotations are well detected even when the phase is prepared from both homeotropically (Figure 2a) and homeogeneously (Figure 2b) aligned nematic phases. On the other hand, for ODBP–OCO-11, which exhibits the SmC phase in a higher-temperature region than the Bx phase, chiral domains are distinguishable only when the sample is cooled from the homeotropically aligned SmC phase (see Figure 3). A similar phenomenon is observed for the Bx phase appearing from the SmA phase in ODBP-8.

ODBP–OCO-*n* and ODBP-8 show high transition temperatures from the calamitic phase to the Bx phase above 200 $^{\circ}$ C. Furthermore, the Bx phase is formed only in the higher-temperature region above 180 $^{\circ}$ C. Hence, X-ray and electrooptic measurements for the Bx phases of these materials are difficult to perform. To obtain better measurement conditions, we

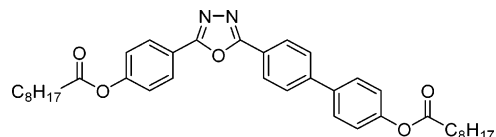


(a) Homeotropic alignment

(b) Homogeneous alignment

Figure 2. POM textures in the Bx phases of ODBP-OCO-8 that are cooled from (a) homeotropically and (b) homogeneously aligned nematic phases. Under cross-polarization, the Bx phases prepared from two differently aligned nematic phases show no birefringence, so that they are optically isotropic. In the left- and right-side photographs observed by rotating of polarizer by $\pm 10^\circ$ from the cross-polarized position, two types of optically active domains with opposite chirality can be seen. The inset in each image indicates the relative positions of the polarizer and analyzer.

prepared the asymmetric material OD(P,BP)-OCO-8, with following formula



Iso 185 °C (3.1) N 181 °C (3.2)
SmC 160 °C (6.6) Bx 69 °C (6.1) Cr

As expected from the equimolar mixture of ODBP-OCO-8 and ODP-OCO-8, this material exhibits a relatively lower T_i of 185 °C. Furthermore, it exhibits the polymorphic transition of Iso-N-SmC-Bx-Cr sequence with a wider temperature range of the Bx phase from 69 to 160 °C. Thus, we can collect detailed information on the orientations of the molecules and layers in the Bx phase by comparison with those in the nematic and SmC phases under more convenient conditions. The average molecular length estimated from the characteristic streak of the nematic liquid crystal is ~ 35 Å, which is nearly equal to the calculated molecular length (35.5 Å). The layer spacing of the SmC phase is 32.1 Å. As observed in other materials, the Bx phase has the same layer spacing as the SmC phase. The tilt angle obtained from a comparison of the layer spacing with the molecular length is about 25 Å for both the SmC and Bx phases.

3.1. POM Observations. Both OD(P,BP)-OCO-8 and ODBP-OCO-n have a tendency to align homeotropically in a sandwich-type cell without any treatment. Hence, we obtained a planar alignment here by using polyimide-coated cells that were uniaxially rubbed. As shown in Figure 4a, the nematic liquid crystals are well aligned with the n-director parallel to the rubbing direction. Upon cooling to the SmC phase, the homogeneous texture is well developed, but two distinct domains with different optical axes (for example, the A and B domains in Figure 4b) are formed. This type of domain structure

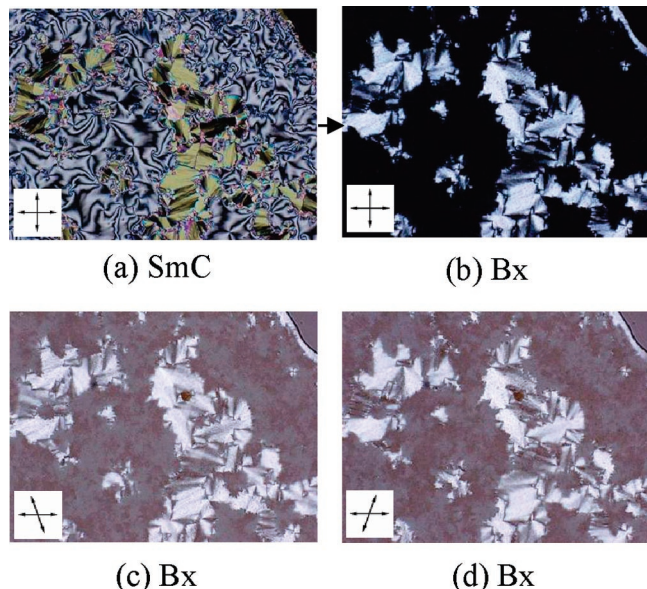


Figure 3. Optical microscopic textures in the (a) SmC phase and (b-d) Bx phase for ODBP-OCO-11: (a,b) cross-polarization, (c,d) rotation of the polarizer by $\pm 10^\circ$ from the cross-polarized position. From b and c, it can be seen that the chiral domain structure is detected only for the Bx phase cooled from the homeotropically aligned SmC phase.

is well-known as the bookshelf structure. The two domains can be more easily recognized by the rotation of the sample stage (see Figure 4c,d); upon a rotation of 10° , domain A becomes completely dark so that the optical axis is parallel to the polarizer direction (Figure 4c), whereas rotation of -10° (Figure 4d) now makes the other B domain dark. Thus, the two kinds of planar domains in the bookshelf structure have averaged molecular axes oppositely tilted by 10° to the rubbing direction. The microbeam X-ray data shown later indicate that the layer normal is tilted by 15° toward the rubbing direction and the molecules within a layer are tilted in a plane parallel to the cell surface. Considering that the tilt angle obtained from a comparison of layer

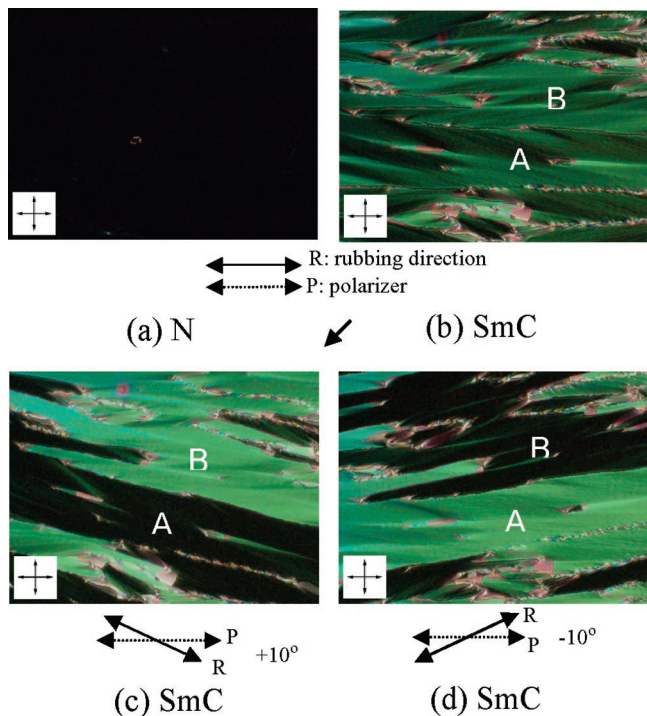


Figure 4. Polarized optical microscopic textures for the SmC phase of OD(P,BP)-OCO-8 aligned by surface anchoring. As seen in b-d, two types of domains, for example, A and B domains, are formed from the homogeneously aligned nematic phase in a. The dark and bright states are switched by rotating the stage, and the bright positions in the A and B domains correspond to the directions making about $+10^\circ$ and -10° angles with respect to the rubbing direction, respectively (see c and d). This means that the long axes of molecules in the SmC phase align in a direction $\pm 10^\circ$ from the rubbing direction.

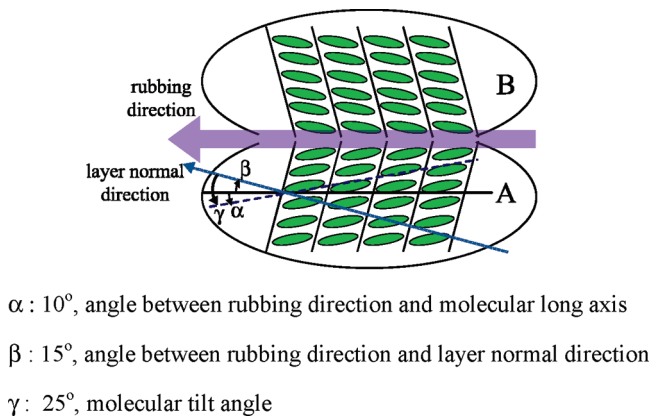


Figure 5. Orientation of layers and molecular arrangements in the two A and B domains of the SmC phase aligned by surface anchoring. spacing and molecular length is 25° , we can reasonably illustrate the layer alignment and molecular orientation within a layer in the bookshelf structure of the SmC phase as in Figure 5.

Of interest is the phenomenon taking place upon cooling to the Bx phase, which is shown in Figure 6. In Figure 6a, one of the two domains of the SmC phase, domain A, is initially placed in such a way that the molecules are oriented along the polarizer in the cross-polarization, i.e., the transmittance light becomes zero. Upon cooling of the sample to the Bx phase, the domain boundaries in the SmC phase are completely retained, but the dark A domain becomes somewhat bright, although the birefringence is remarkably decreased (see Figure 6b). Then, we tried to rotate the sample stage to obtain zero transmittance for the A domain of the Bx phase. The resulting rotation angle was about -25° (Figure 6c). Precisely the same phenomenon can

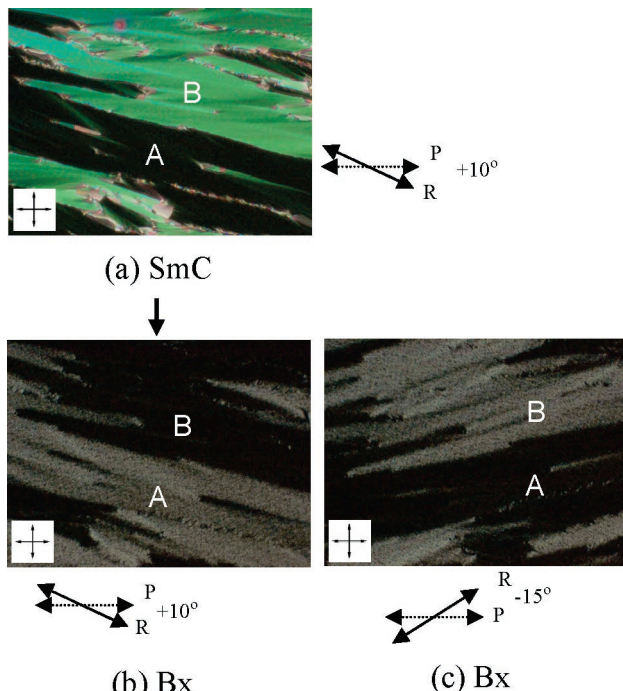


Figure 6. Polarized optical microscopic textures showing the change of the intensity of the transmitted light in domain A upon the transition of the (a) SmC phase to the (b,c) Bx phase. Initially, the sample stage is set at the extinction position such that domain A of the SmC phase becomes most dark (see a). Upon cooling to the Bx phase, the domain structure is completely retained as found in b, but the transmittance light of domain A is relatively increased. Then, the new extinction position of domain A can be attained by rotating the stage by 25° (see c). By the same procedure, the extinction position of domain B can be achieved by a sample stage rotation of -25° . This means that the Bx phase is birefringent and its optical axis is almost parallel to the layer normal direction of the preceding SmC layer.

be detected for the B domain by rotating the stage by +25°. This rotation angle corresponds to the tilt angle of the molecules to the layer normal in the SmC phase. Thus, we obtain an important fact that the Bx phase has a certain optical axis lying along the layer or layer normal of the preceding SmC phase.

Similar microscopic observations were made for the SmA-Bx phase transition in ODBP-8. In the SmA phase, the molecular axis and then the optical axis correspond to the rubbing direction. Upon the transformation to the Bx phase, the birefringence becomes weak, but the optical axis in the Bx phase remains unchanged, leading to the same conclusion that optical axis of the Bx phase lies along the layer or layer normal.

When the Bx phase is formed from the homeotropically aligned SmC or SmA phase, it appears optically isotropic under cross-polarization. The texture is thus featureless in this case, but two clear domains with opposite optical rotations can be detected by the rotation of polarizer from the perfectly crossed position as stated above.

3.2. X-ray Measurements. X-ray measurements provide an exclusive characteristic for the Bx phase structure. First, we performed X-ray measurements with two different irradiation geometries for the homeotropically aligned sample on a glass plate treated with organosilane, as stated in the Experimental Section: one is with the incident X-ray beam parallel to glass substrate (i.e., parallel to the layer plane of SmC phase), whereas the other is normal to the substrate. Figure 7 presents X-ray photographs taken for the SmC and Bx phases in these two geometries.

For the parallel incidence, we observe two SmC layer reflections along the meridian line (see Figure 7a), which is

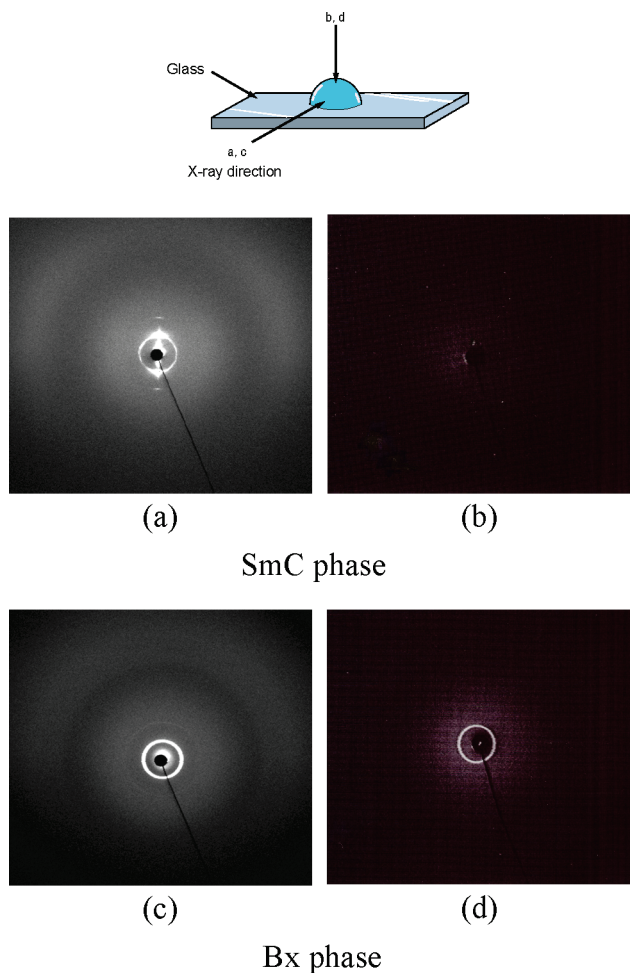


Figure 7. Typical WAXD patterns recorded for (a,b) the SmC phase homeotropically aligned on the glass by surface treatment and (c,d) the resulting Bx phase in OD(P,BP)-OCO-8. a and c were recorded with the incidence parallel to the glass surface, whereas b and d were recorded with the incidence normal to the glass surface.

expected from the homeotropic alignment of layers. Upon cooling of the sample to the Bx phase, a dramatic change in the reflection profile takes place: the oriented pattern is completely smeared to result in a ring pattern (Figure 7c). This means that the homeotropic alignment of the layers in the SmC phase is completely lost and the layer normal of the Bx phase is randomly displaced with respect to the glass surface. The same result can be obtained with normal incidence to the layer: no layer reflection is observed for the SmC phase, whereas such a reflection clearly appears upon transformation to the Bx phase (compare parts b and d of Figure 7). This result coincides with the findings of Weissflog et al.,³⁸ who reported that the orientation in the higher-temperature nematic phase disappeared upon cooling to the lower-temperature X phase. A similar disorientation of layers was reported to take place upon the B2-B4 phase transition of P-n-O-PIMB by Thisayukta et al.¹⁸

To clarify this disorientation more extensively, a micro-X-ray beam measurement was performed for the SmC-Bx phase transition in the same planar aligned sample as treated for the POM measurements in Figure 6. The X-ray pattern in Figure 8a was observed with a microbeam radiated into a single A domain of the SmC phase. A spotted pair of oriented layer (inner) reflections can be observed in a direction making an angle of 15° toward the equatorial line (i.e., the rubbing direction). On the other hand, the outer broad reflection

indicating the liquidlike packing of molecules within a layer appears in a direction making an angle of 65–68° to the layer reflection. This means that the molecules are tilted with respect to the layer at a tilt angle of 22–25°, which nearly corresponds to the 25° value determined from the comparison of the layer spacing and the molecular length. The X-ray patterns of Figure 8b obtained by the irradiation of domain B are the same as those in domain A, but they are symmetrical with respect to the rubbing direction. Thus, the X-ray data satisfy the structural model of Figure 5 deduced from the POM observation.

Again, tremendous changes can be seen here upon cooling to the Bx phase. The oriented X-ray pattern changes to a ring pattern (see Figure 8c,d). Thus, it can be concluded that the disorientation of the layers takes place even in a single domain.

3.3. Electrooptic Measurements. We performed electrooptic measurements in the Bx phase for OD(P,BP)-OCO-8. The sample was filled into a sandwiched ITO-coated glass cell (5-μm cell gap) with a planar alignment treatment. A relatively high voltage was required for the optically isotropic Bx phase to show an electrooptic response. Upon application of a triangular voltage of 10 Hz and 80 Vpp, the Bx phase shows a texture transformation and simultaneously two switching current peaks (see Figure 9) within a half-period. Thus, the antiferroelectric response is obvious. The spontaneous polarization is around 600 nC cm⁻².

The field-induced texture is a brilliant grainy texture that exhibits a birefringence somewhat higher than that of the original state, as shown in Figure 10. It should be noted that the integral of the current peaks increases as the birefringent area grows. This means that the antiferroelectric switching response could be attained after a textural transformation.

When the field is continuously applied, the texture is developed to a relatively large size. For this developed texture, we can recognize that extinction brushes rotate and birefringent color changes upon application of a dc voltage. These are distinct characteristics of a homochiral domain. The rotation angle that corresponds to the tilt angle is 20–25°. This value is in good agreement with that estimated from optical microscopy and X-ray observations. Thus, we conclude that the field-induced phase is regarded as the B2 phase with homochiral SmC_{AP} structure.

The resulting B2 phase remains stable at temperatures 20 °C or more lower than the Bx-SmC transition. However, if it is reheated to the temperature near the transition to the SmC phase, it returns back to the weakly birefringent Bx phase.

4. Discussion. Optically isotropic and chiral phases have been reported in various banana molecular systems. To what are these phases assigned? One candidate is the well-known B2 phase with the SmC_{AP} layer structure. To explain the optically isotropic and chiral features, Ortega et al.³⁷ considered a SmC_{AP} layer structure with small domains; their random orientation could give rise to an optically isotropic state, and antiferroelectric and reverse-tilted molecules in adjacent layers could form a chiral layer structure with a periodicity of two layers such as a short-pitch SmC*-type structure. Furthermore, recently a layer optical chirality (LOC) model was developed for the tilted B2 phase in the absence of a superlayer helix.⁴⁰

In our case, the results of X-ray and optical microscopic measurements indicate that the Bx phase has a very complicated layer structure. The results obtained for the Bx phase can be summarized as follows:

- (1) The Bx phase is optically isotropic or very weakly birefringent when it is formed from the homeotropically aligned SmC and SmA layer phases. By the rotation of a polarizer, two

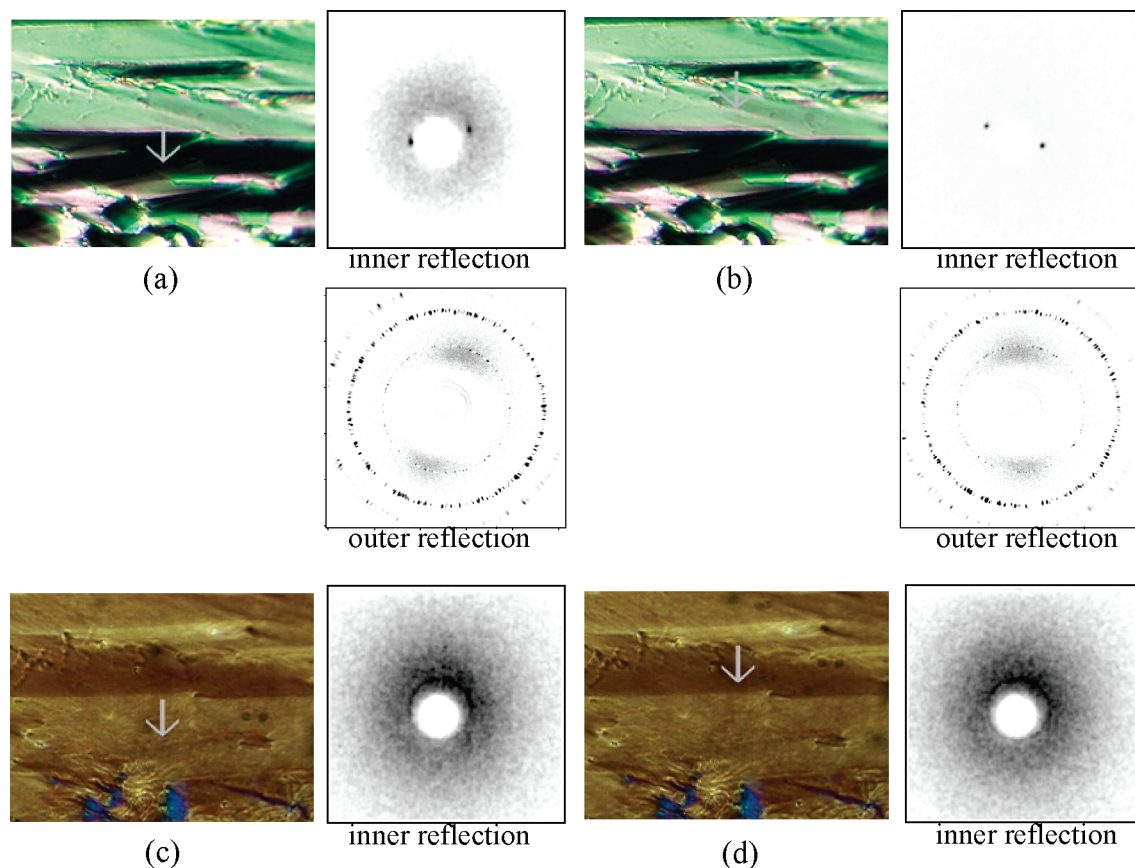


Figure 8. X-ray patterns of (a,b) the SmC phase and (c,d) the Bx phase taken by the microbeam. Here, the microbeam was irradiated onto domains A and B of the same sample as in Figure 6. The horizontal direction corresponds to the rubbing direction.

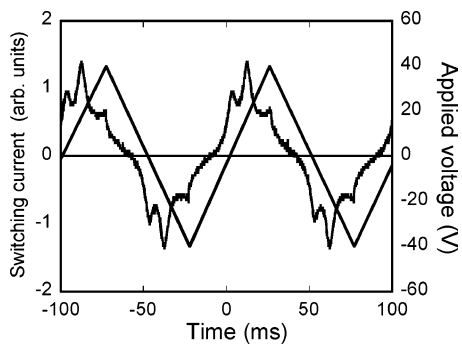


Figure 9. Reversal current responses to the applied triangular waveform on the Bx phase of OD(P,BP)-OCO-8, showing two peaks within the half-cycle that are characteristic of an antiferroelectric nature. A capacitor-type 5- μm cell with planar alignment was used under conditions of 80 Vpp and 10 Hz.

chiral domains with opposite optical rotations can be detected. On the other hand, the Bx phase appearing from the homogeneously aligned smectic phases exhibits a weak but well-defined birefringence. Its optical axis lies along the layer or layer normal of the preceding smectic phase.

(2) The Bx phase exhibits an X-ray pattern with sharp inner and outer broad reflections similarly to the SmA and SmC phases. The layer spacings are similar to those of the SmC phase, and the estimated tilt angles are 25–35°. The remarkable fact obtained from X-ray observations is that the complete disorientation of the layers takes place upon cooling from the oriented SmA or SmC phase.

(3) The Bx phase is transformed to the well-known B2 phase when an electric field larger than 8 V μm^{-1} is applied to the homogeneously aligned cell. The field-induced B2 phase

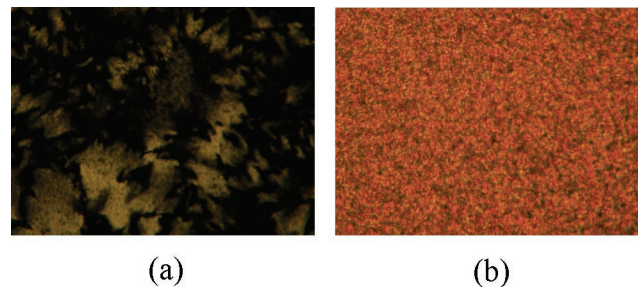


Figure 10. POM textures of the Bx phase at (a) $E = 0$ state and (b) $E = \text{on}$ state for OD(P,BP)-OCO-8. At the initial state of $E = 0$, the Bx phase shows very weak birefringence (a). By applying external voltages over E_{th} (threshold voltage), an antiferroelectric switching behavior is observed, and simultaneously the texture transformation occurs in the entire area. The resulting texture is grainy, but highly birefringent (b).

exhibits a homochiral SmCAPA structure. It remains at temperatures by 20 °C or more lower than the transition to the SmC phase, but it transforms in to the Bx phase near the transition temperature.

All of these results simply indicate that the Bx phase results as a frustration (or disorientation of layers) from the ground-state B2 phase. What kind of frustration has taken place in the B2 phase? A key fact to answer this question is the weak birefringence observed even after the disorientation of the layers from the homogeneously aligned SmC phase as seen in Figure 6. The extinction direction is along the layer and layer normal, meaning that the disorientation of the layers takes place not randomly, but with a certain optical axis. This distinct feature can be satisfied only by a helical twisting model such as the twisted grain boundary (TGB) structure with small layer blocks that are twisted from each other along the layer of the preceding

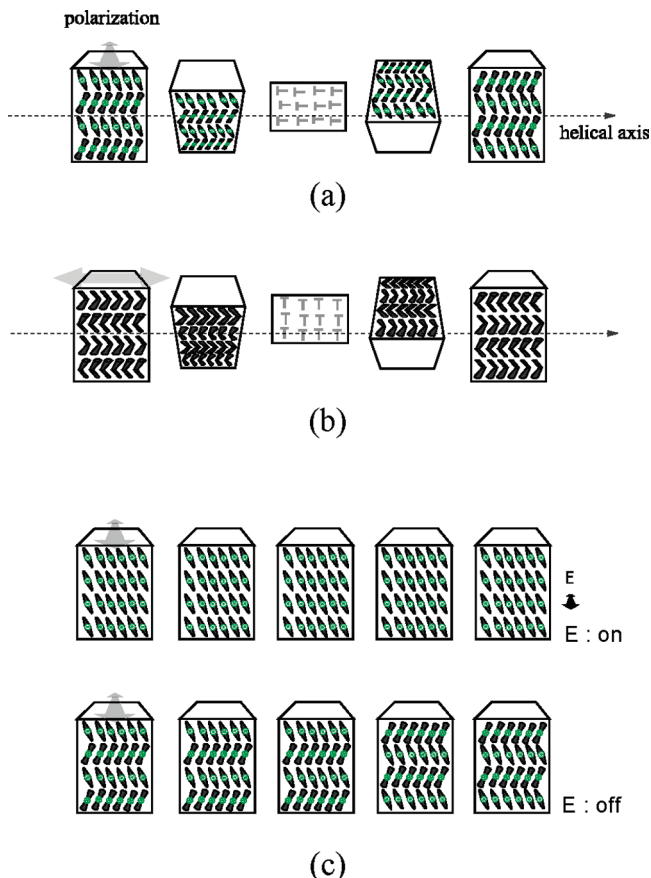


Figure 11. (a,b) Illustration of two possible structural models with helical deformation of the layer blocks. In each block, molecules are packed in an anticlinic and antiferroelectric manner. (c) Under the application of a sufficient external field, the helical structure is unwound to produce the ground-state B2 layer structure.

smectic phases because the helicoidal structure behaves as a uniaxial crystal with the optical axis along the helix axis and apparently causes the disorientation of the layers. In fact, a TGB-like structure was discussed by Jákli et al. to explain an optically isotropic and chiral smectic phase with a model in which the helical axis is lying parallel to the incidence direction of visible light.³⁶

Because the SmC phase is biaxial, two helical axes along the layer, parallel and perpendicular to the tilt plane, are possible, as illustrated in Figure 11a and b, respectively. First, we consider the helical twisting occurring parallel to the tilt direction. This model can explain the birefringence in the microscopic observations of Figure 6, but not the disorientation in the X-ray pattern of Figure 8 because the layer normal of any layer block is within a plane parallel to the beam direction. In contrast, the second model with the helical axis lying perpendicular to the tilt direction can satisfy the X-ray pattern of Figure 8, but cannot explain the remaining birefringence seen in Figure 6. Thus, we reach the suggestion that there is no preferred in-plane direction of the helical twisting; in other words, the helical twisting takes place along both axes.

We next refer to the fact that the chiral domains are clearly recognized only in a homeotropic view. If our helical twisting model is correct, this fact means that the optical activity in a direction perpendicular to the helical axis is more predominant than that along the helical axis. In principle, this is surprising because the de Vries formula indicates that optical rotations along the helical axis should be significant.⁴¹ According to a recent report by Ortega et al.,³⁷ however, the optical rotation

along the helical axis scales as $(P/\lambda)^3$, whereas that perpendicular to the helical axis scales as (P/λ) . Here, P and λ are the helical pitch and wavelength of light, respectively. Thus, the predominant optical activity along the helical axis observed here suggests that the helical pitch might be smaller than the wavelength. In this respect, it should be noted that the B4 phase of the classical P-12-O-PIMB with the similar helical structure shows chiral domain structures only when it is prepared from the homogeneously aligned B2 phase.¹⁸ Hence, in the B4 phase, the helical pitch is considered to be comparable to or larger than the wavelength of light.

Finally, we state that the field-induced B2 phase is caused by the simple unwinding of the helix of Bx phase as observed in the TGB_C phase formed from chiral rodlike molecules.⁴²

Conclusions

Banana-shaped molecules based on the oxadiazole core whose bend angle is slightly larger than that of the conventional P-n-O-PIMB were prepared, and their mesomorphic properties were investigated by taking notice of the banana phase.

The oxadiazole derivatives exhibit a liquid-crystal polymorphism showing both the calamitic and banana Bx phases. The Bx phase has a layered structure in which the molecules are packed with a liquidlike nature and are tilted with respect to the layer. The phase is thus similar to the first observed conventional B2 phase, but it can be different in the respect that it is optically chiral and weakly birefringent. These specific structural features of the Bx phase were examined in detail in relation to the structures of calamitic liquid crystals. The most distinct result obtained is that the disorientation of the layers takes place upon the transformation to the Bx phase from the well-oriented calamitic phase. Irrespective of this disorientation, the Bx phase has an optical axis parallel to the layer plane of the preceding smectic phase. To explain both results, we reach the conclusion that the Bx phase has a TGB-like helical structure as is observed in the B4 phase. The induction of the B2 phase from the Bx phase by application of an external electric field shows that the helical twisting of the Bx phase is produced from the ground-state B2 phase with the homochiral SmC_{AP} structure.

References and Notes

- (1) Vorländer, D. *Ber. Dtsch. Chem. Ges.* **1929**, 62, 2831.
- (2) Demus, D. *Liq. Cryst.* **1989**, 5, 75.
- (3) Kuboshita, M.; Matsunaga, Y. *Mol. Cryst. Liq. Cryst.* **1991**, 199, 319.
- (4) Matsuzaki, H.; Matsunaga, Y. *Liq. Cryst.* **1993**, 14, 105.
- (5) Akutagawa, T.; Matsunaga, Y.; Yasuhara, K. *Liq. Cryst.* **1994**, 17, 659.
- (6) Watanabe, J.; Hayashi, M. *Macromolecules* **1988**, 21, 278; *Macromolecules* **1989**, 22, 4083.
- (7) Watanabe, J.; Kinoshita, S. *J. Phys. II (Fr.)* **1992**, 2, 1273.
- (8) Watanabe, J.; Hayashi, M.; Nakata, Y.; Niori, T.; Tokita, M. *Prog. Polym. Sci.* **1997**, 22, 1053.
- (9) Nakata, Y.; Shimizu, K.; Watanabe, J. *J. Phys. II (Fr.)* **1994**, 4, 581.
- (10) Nakata, Y.; Watanabe, J. *Polym. J.* **1997**, 29, 193.
- (11) Niori, T.; Adachi, S.; Watanabe, J. *Liq. Cryst.* **1995**, 19, 139.
- (12) Watanabe, J.; Izumi, T.; Niroi, T.; Zen-nyojoji, M.; Takanishi, Y.; Takezoe, H. *Mol. Cryst. Liq. Cryst.* **2000**, 346, 77.
- (13) Watanabe, J.; Niori, T.; Choi, S. W.; Takanishi, Y.; Takezoe, H. *Jpn. J. Appl. Phys.* **1998**, 37, 401.
- (14) Niori, T.; Sekine, T.; Watanabe, J.; Furukawa, T.; Takezoe, H. *J. Mater. Chem.* **1996**, 6, 1231.
- (15) Sekine, T.; Niori, T.; Sone, M.; Watanabe, J.; Takanishi, Y.; Choi, S. W.; Takezoe, H. *Jpn. J. Appl. Phys.* **1997**, 36, 6455.
- (16) Link, D. R.; Natale, G.; Shao, R.; MacLennan, J. E.; Clark, N. A.; Körblova, E.; Walba, D. M. *Science* **1997**, 278, 1924.
- (17) Heppke, G.; Moro, D. *Science* **1998**, 279, 1872.

- (18) Thisayukta, J.; Takezoe, H.; Watanabe, J. *Jpn. J. Appl. Phys.* **2001**, *40*, 3277.
- (19) Pelzl, G.; Diele, S.; Weissflog, W. *Adv. Mater.* **1999**, *11*, 707.
- (20) Semmler, Klaus J. K.; Dingemans, T. J.; Samulski, E. T. *Liq. Cryst.* **1998**, *24*, 799.
- (21) Dingemans, T. J.; Samulski, E. T. *Liq. Cryst.* **2000**, *27*, 131.
- (22) Acharya, B. R.; Primak, A.; Kumar, A. *Phys. Rev. Lett.* **2004**, *92*, 145506.
- (23) Madsen, L. A.; Dingemans, T. J.; Nakata, M.; Samulski, E. T. *Phys. Rev. Lett.* **2004**, *92*, 145505.
- (24) Dingemans, T. J.; Sanjeeva Murthy, N.; Samulski, E. T. *J. Phys. Chem. B* **2001**, *105*, 8845.
- (25) Weissflog, W.; Nádası, H.; Dunemann, U.; Pelzl, G.; Diele, S.; Eremin, A.; Kresse, H. *J. Mater. Chem.* **2001**, *11*, 2748.
- (26) Amaranatha Reddy, R.; Sadashiva, B. K.; Dhara, S. *Chem. Commun.* **2001**, *19*, 1972.
- (27) Thisayukta, J.; Nakayama, Y.; Kawauchi, S.; Takezoe, H.; Watanabe, J. *J. Am. Chem. Soc.* **2000**, *122*, 7441.
- (28) Dantlgraber, G.; Eremin, A.; Diele, S.; Hauser, A.; Kresse, H.; Pelzl, G.; Tschiertske, C. *Angew. Chem., Int. Ed.* **2002**, *41*, 2408.
- (29) Pelzl, G.; Eremin, A.; Diele, S.; Kresse, H.; Weissflog, W. *J. Mater. Chem.* **2002**, *12*, 2591.
- (30) Huang, M. Y. M.; Pedreira, A. M.; Martins, O. G.; Figueiredo Neto, A. M.; Jákli, A. *Phys. Rev. E* **2002**, *66*, 031708.
- (31) Shreenivasa Murthy H. N.; Sadashiva, B. K. *Liq. Cryst.* **2002**, *29*, 1223.
- (32) Pyc, P.; Mieczkowski, J.; Pociecha, D.; Gorecka, E.; Donnio, B.; Guillou, D. *J. Mater. Chem.* **2004**, *14*, 2374.
- (33) Eremin, A.; Diele, S.; Pelzl, G.; Weissflog, W. *Phys. Rev. E* **2003**, *67*, 020702.
- (34) Etxebarria, J.; Folcia, C. L.; Ortega, J.; Ros, M. B. *Phys. Rev. E* **2003**, *67*, 042702.
- (35) Fodor-Csorba, K.; Vajda, A.; Galli, G.; Jákli, A.; Demus, D.; Holly, S.; Gács-Baitz, E. *Macromol. Chem. Phys.* **2002**, *203*, 1556.
- (36) Jákli, A.; Huang, Y.-M.; Fodor-Csorba, K.; Vajda, A.; Galli, G.; Diele, S.; Pelzl, G. *Adv. Mater.* **2003**, *15*, 1606.
- (37) Ortega, J.; Folcia, C. L.; Etxebarria, J.; Gimeno, N.; Ros, M. B. *Phys. Rev. E* **2003**, *68*, 011707.
- (38) Weissflog, W.; Sokolowski, S.; Dehne, H.; Das, B.; Grande, S.; Schröder, M. W.; Eremin, A.; Diele, S.; Pelzl, G.; Kresse, H. *Liq. Cryst.* **2004**, *31*, 923.
- (39) Liao, G.; Stojadinovic, S.; Pelzl, G.; Weissflog, W.; Sprunt, S.; Jákli, A. *Phys. Rev. E* **2005**, *72*, 021710.
- (40) Hough, L. E.; Clark, N. A. *Phys. Rev. Lett.* **2005**, *95*, 107802.
- (41) de Vries, H. *Acta Cryst.* **1951**, *4*, 219.
- (42) Meier, J. G.; Rudquist, P.; Petrenko, A. S.; Goodby, J. W.; Lagerwall, S. T. *Liq. Cryst.* **2002**, *29*, 179.